Constraints on the lower mantle electrical conductivity: limitations on Backus mantle filter theory and the inverse problem.

Pinheiro, K.J.[1], Jackson, A.[2], Velímský, J.[3],

[1]National Observatory- Rio de Janeiro, [2]ETH-Zurich, [3]Chales University- Prague

Abstract

In this paper we constrain the electrical conductivity of the lower mantle is by using geomagnetic jerks that are abrupt changes in the secular variation generated in the core. By appling Backus' (1983) mantle filter theory it is possible to show that a simple 1D mantle conductivity model is able to generate differential delays. However, Backus's (1983) theory considers a low frequency approximation of the transfer function that presents some limitations. We also calculate of the Impulse Response Function (IRF) by a modified version of Velmský and Martinec's (2005) code, using a direct time-integration of the EM induction equation. The inverse problem was solved, by exhaustive search. The misfit values for all simulations, favour a low conductivity of the lower mantle of about 1 S/m.

Introduction

The mantle electrical conductivity can be analysed by experimental and theoretical mineral physics, induction studies that use variations of the external magnetic field, also using time variations of the core magnetic field. Most results agree on 1D models of the mantle electrical conductivity, from about 300 to 1000 km depth, but below that the electrical conductivity is mostly unknown, besides the recent efforts of mineral physics experiments. We use time variations of the core magnetic field in the attempt to obtain constraints on the mantle electrical conductivity. Geomagnetic jerks are abrupt changes in the secular variation generated in the core, represented by an impulse in the n^{th} time derivative of the magnetic field (Figure 1).

In this paper, we assume that the secular variation around the time of geomagnetic jerks can be modelled by a set of straight line segments and that the point where the lines intersect defines the occurrence time of the geomagnetic jerk. The difference between the slope of consecutive straight lines defines the jerk amplitude at each location; these are used to build spherical harmonic models of each jerk in each field component.

Global jerks occurred at different epochs: 1969, 1978, 1991, while some localised events happened in 1913, 1925 and 2003 (Alexandrescu *et al.* (1996), Michelis & Tozzi (2005), Mandea *et al.* (2000), Nagao *et al.* (2002), Olsen & Mandea (2007)). Each of the worldwide jerks presents a different geographical pattern of early and late jerks arrivals, with differential time delays of the order of 2 years. For instance, the 1969 and 1978 jerks were detected roughtly first in Northern hemisphere and later in Southern observatories. Pinheiro & Jackson (2008) applied Backus' (1983) mantle filter theory and concluded that a simple 1D mantle conducting model is able to generate differential jerk time delays at the Earth's surface and even different patterns for different jerk events. We also showed that the delay patterns depend strongly on the mantle electrically conducting model considered and on the jerk morphology at the CMB.

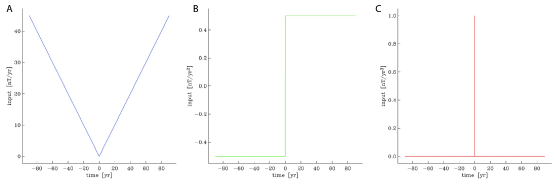

Figure 1: Simple schematic of secular variation for a hypothetical component of the magnetic field that are used as input in the forward and inverse problems. The first graph (A) shows the typical V-shape of jerks in the secular variation and B and C show sketched the secular acceleration and the third differences, respectively. In this case, we would have an impulse in the third differences at the time when the jerk occurred.

On the Limitations of Backus Filter Theory

Backus (1983) developed a theory that considers the mantle as a linear, causal and time invariant filter. In what follows we adopt the separation by spherical harmonic degree ℓ, any output at the Earth's surface ($r = a$, $p_\ell^m(a,t)$) can be calculated by the convolution between the input at the CMB ($r = c$, $(p_\ell^m(c,t))$) and the electromagnetic ($F_\ell(t)$) and geometrical ($\mathscr{G}_\ell$) filters:

$$\begin{aligned} p_\ell^m(a,t) &= \mathscr{G}_\ell F_\ell(t) * p_\ell^m(c,t) \\ &= \mathscr{G}_\ell \int_{-\infty}^{\infty} F_\ell(t-t') p_\ell^m(c,t') dt'. \end{aligned} \quad (1)$$

The input jerk is assumed as a simultaneous second order impulse at the CMB (Figure 1), represented by $\delta \ddot{p}_\ell^m(c,t) = \delta(t)$, where $\delta(t)$ is a Dirac delta. The output can be written as

$$\begin{aligned} \delta \ddot{p}_\ell^m(a,t) &= \mathscr{G}_\ell \int_{-\infty}^{\infty} F_\ell(t-t') \delta(t') dt' \\ &= \mathscr{G}_\ell F_\ell(t), \end{aligned} \quad (2)$$

where $F_\ell(t)$ is called the *Impulse Response Function (IRF)* that characterizes the mantle filter depending on its electrical conductivity.

The Fourier transform of the IRF,

$$\tilde{F}_\ell(\omega) = \int_{-\infty}^{\infty} F_\ell(t) e^{\imath\omega t} dt, \tag{3}$$

is called the *Transfer Function (TF)* and for zero frequency $\omega = 0$,

$$\tilde{F}_\ell(0) = \int_{-\infty}^{\infty} F_\ell(t) dt, \tag{4}$$

which is the area under the IRF curve for each harmonic degree ℓ. We use the same convention as Backus (1983) in which $\int_{-\infty}^{\infty} F_\ell(t)dt = 1$.

Backus (1983) assumes a low frequency approximation, where higher powers than frequency ω^2 are neglected in the series expansion of the Transfer Function. This assumption simplifies Backus' (1983) mantle filter theory, since the IRF can be represented by a Gaussian, and it leads to a linear relationship between the mantle electrical conductivity and the time an impulse takes to pass through the conducting mantle.

In order to demonstrate this low frequecy approximation, we start from Backus'(1983) equation 2.2:

$$\tilde{F}(\omega) = \tilde{F}(0) \sum_{n=0}^{\infty} \frac{1}{n!} (\imath\omega\tau_n)^n, \tag{5}$$

where τ_n^n are called the nth ordinary moments, given by

$$(\tau_n)^n = \frac{1}{\tilde{F}(0)} \int_{-\infty}^{\infty} F(t) t^n dt. \tag{6}$$

and $(\beta_n)^n$ the nth central moments:

$$(\beta_n)^n = \frac{1}{\tilde{F}(0)} \int_{-\infty}^{\infty} F(t)(t-\tau_1)^n dt. \tag{7}$$

Since the TF can be expressed by the Fourier transform of the IRF (shown in equation 3), we have:

$$\begin{aligned}
\tilde{F}(\omega) &\approx \int_{-\infty}^{\infty} F(t) e^{\imath\omega t} dt \\
&= \int_{-\infty}^{\infty} F(t) \sum_{n=0}^{\infty} \frac{1}{n!} (\imath\omega t)^n dt \\
&= \int_{-\infty}^{\infty} F(t) dt + \imath\omega \int_{-\infty}^{\infty} F(t) t dt \\
&- \frac{\omega^2}{2} \int_{-\infty}^{\infty} F(t) t^2 dt - \frac{\imath\omega^3}{6} \int_{-\infty}^{\infty} F(t) t^3 dt + ... \\
&= \tilde{F}(0) + \tilde{F}(0)\imath\omega\tau_1 - \tilde{F}(0)\frac{\omega^2}{2}\tau_2^2 - \tilde{F}(0)\frac{\imath\omega^3}{6}\tau_3^3 + (8)
\end{aligned}$$

and if we truncate this expansion at ω^2, the TF is rewritten by

$$\tilde{F}(\omega) = \tilde{F}(0) \left[1 + \imath\omega\tau_1 - \frac{\omega^2}{2}\tau_2^2 \right]. \tag{9}$$

A simple expansion of equation 7 shows that the central moments can be expressed in terms of ordinary moments; we find

$$\beta_2^2 = \tau_2^2 - \tau_1^2, \tag{10}$$

and substituting τ_2^2 from equation 10, in equation 9, we have

$$\begin{aligned}
\tilde{F}(\omega) &\approx \tilde{F}(0) \left[1 + \imath\omega\tau_1 - \frac{\omega^2}{2} \left(\tau_1^2 + \beta_2^2 \right) \right] \\
&\approx \tilde{F}(0) e^{\imath\omega\tau_1 - \frac{\beta_2^2}{2}\omega^2}.
\end{aligned} \tag{11}$$

In order to calculate the IRF, we take the inverse Fourier transform of equation 11:

$$\begin{aligned}
F(t) &= \frac{1}{2\pi} \int_{-\infty}^{\infty} \tilde{F}(\omega) e^{-\imath\omega t} d\omega \\
&= \frac{\tilde{F}(0)}{2\pi} \int_{-\infty}^{\infty} e^{\imath\omega(\tau_1 - t) - \frac{\beta_2^2}{2}\omega^2} d\omega \\
&= \frac{\tilde{F}(0)}{2\pi} \sqrt{\frac{2\pi}{\beta_2^2}} \quad e^{-\frac{(\tau_1 - t)^2}{2\beta_2^2}} \\
&= \frac{\tilde{F}(0)}{\beta_2\sqrt{2\pi}} \quad e^{-\frac{(\tau_1 - t)^2}{2\beta_2^2}},
\end{aligned} \tag{12}$$

where $\frac{F(t)}{\tilde{F}(0)}$ has the form of a Gaussian with mean τ_1, given by the first ordinary moment ($n = 1$ in equation 6)

$$\tau_1 = \frac{1}{\tilde{F}(0)} \int_{-\infty}^{\infty} F(t) t dt \tag{13}$$

and called the *delay time*, which is the time an impulse at the CMB takes to pass through the conducting mantle. In equation 12, β_2^2 is the variance, called the *smoothing time* and given by the second central moment ($n = 2$ in equation 7)

$$\beta_2^2 = \frac{1}{\tilde{F}(0)} \int_{-\infty}^{\infty} F(t)(t - \tau_1)^2 dt. \tag{14}$$

If one aims to calculate the delay and smoothing time constants for each harmonic degree, equations 13 and 14 become:

$$\tau_1(\ell) = \int_{-\infty}^{\infty} F_\ell(t) t dt. \tag{15}$$

and

$$(\beta_2(\ell))^2 = \int_{-\infty}^{\infty} F_\ell(t) \left(t - \tau_1(\ell)\right)^2 dt, \tag{16}$$

since $\tilde{F}_\ell(0) = 1$ (equation 4). In order to illustrate the effect of the electrical conducting mantle, we used two radial conductivity models, given by:

$$\sigma(r) = \sigma_c \left(\frac{c}{r} \right)^{2\gamma+2}, \tag{17}$$

where σ_c is the electrical conductivity at the CMB, γ a positive constant and $r = c$ is the core radius. Using equation 17 we calculate the IRFs and TFs.

The delay and smoothing time constants were evaluated, by equations 13 - 16, for two radial models. These examples, illustrated in Figure 2, show that higher conductivity models and lower spherical harmonic degrees generate more delayed and usually more smoothed outputs. It is possible to compare, in Figure 2, the delay time of the different models and spherical harmonic degrees: for the most conducting model $\tau_1(1) = 2.57$ yr and for $\ell = 5$ the delay time is smaller ($\tau_1(5) = 1.99$ yr), while for

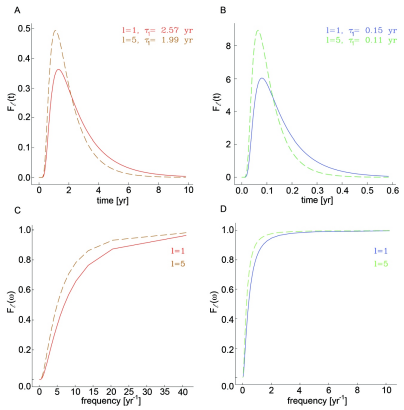

Figure 2: Impulse Response Functions (A, B) and Transfer Functions (C, D) for the two radial electrical conductivity models, shown in equation 17. Plots A and C correspond to the higher conducting model ($\sigma_c = 3000$ and $\gamma = 11$) while plots B and D correspond to the weaker conducting model ($\sigma_c = 100$ and $\gamma = 8$).

the less conducting model $\tau_1(1) = 0.15$ yr and $\tau_1(5) = 0.11$ yr.

We note that every spherical harmonic component of the poloidal scalar travels independently through the mantle. We introduce our simple model for the jerk at the CMB, namely

$$\delta \ddot{p}_\ell^m(c,t) = \mathscr{G}_\ell^{-1} \delta \ddot{p}_\ell^m(a) \delta(t). \tag{18}$$

and at the Earth's surface the output is

$$\delta \ddot{p}_\ell^m(a,t) = \delta \ddot{p}_\ell^m(a) F_\ell(t). \tag{19}$$

The matching conditions between an insulator and a conductor give two representations at the Earth's surface:

$$\mathbf{B} = -\nabla V \tag{20}$$

with

$$V = a \sum_{\ell=1}^{L} \sum_{m=0}^{\ell} B_\ell^m Y_\ell^m \tag{21}$$

and for the conductor

$$\mathbf{B} = \nabla \times \nabla \times \mathscr{P}\mathbf{r}, \tag{22}$$

where the relationship between the two is

$$B_\ell^m = -\frac{\ell p_\ell^m}{a}. \tag{23}$$

We now illustrate Backus' phenomenon of mode mixing in different locations correspondent to magnetic observatories, and in different components (X, Y and Z). Backus (1983) expresses the magnetic components in terms of the poloidal scalar by a spherical harmonic expansion:

$$X(r,\theta,\phi,t) = \sum_{\ell=1}^{\infty} \sum_{m=-\ell}^{\ell} \frac{\partial Y_\ell^m(\theta,\phi)}{\partial \theta} B_\ell^m(r,\theta,\phi), \tag{24}$$

$$Y(r,\theta,\phi,t) = -\sum_{\ell=1}^{\infty} \sum_{m=-\ell}^{\ell} \csc\theta \frac{\partial Y_\ell^m(\theta,\phi)}{\partial \phi} B_\ell^m(r,\theta,\phi), \tag{25}$$

and

$$Z(r,\theta,\phi,t) = \sum_{\ell=1}^{\infty} \sum_{m=-\ell}^{\ell} (\ell+1) Y_\ell^m(\theta,\phi) B_\ell^m(r,\theta,\phi), \tag{26}$$

where $Y_\ell^m(\theta,\phi)$ are the spherical harmonics. Alternatively to equation 18 one can imagine that the impulse is in the radial component, given by

$$\delta \ddot{B}_r(c,\theta,\phi,t) = -\frac{1}{c} \sum_{\ell=1}^{\infty} \sum_{m=-\ell}^{\ell} \ell(\ell+1) \delta \ddot{p}_\ell^m(c) \delta(t) Y_\ell^m(\theta,\phi). \tag{27}$$

If the input in the poloidal field is a second order impulse and a given jerk morphology is considered at a given location (θ_0 is the colatitude and ϕ_0 the longitude) at the Earth's surface ($r = a$), we find for B_r

$$\begin{aligned} \delta \ddot{B}_r(a,\theta_0,\phi_0,t) &= \sum_{\ell=1}^{L} \int_{-\infty}^{\infty} -\mathscr{A}_\ell(r,\theta_0,\phi_0) F_\ell(t-t') \delta(t') dt' \\ &= \sum_{\ell=1}^{L} \mathscr{A}_\ell(r,\theta_0,\phi_0) F_\ell(t) \\ &= F(r,\theta_0,\phi_0,t) \end{aligned} \tag{28}$$

where $F(r,\theta_0,\phi_0,t)$ is called the *Composite Impulse Response Function (CIRF)*. We have for $B_r(a,\theta_0,\phi_0)$

$$\mathscr{A}_\ell^m(a,\theta_0,\phi_0) = -(\ell+1) Y_\ell^m B_\ell^m \tag{29}$$

that simply represent the spherical harmonic components of the amplitude (or morphology) of the jerk at the Earth's surface, as shown in Figure 3 for the Y component of the 1969 jerk.

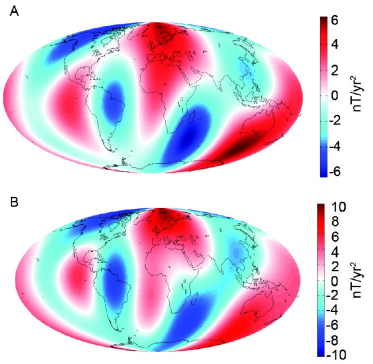

Figure 3: Spherical harmonic models of the 1969 jerk amplitudes calculated in this work (A) with truncation degree $L = 5$ and by Le Huy *et al.* (1998) (B) with truncation degree $L = 4$.

If one wants to calculate the delay time in different locations at the surface, one may use equation 13 but for the CIRF instead of the IRF:

$$\begin{aligned} \tau_1(r,\theta_0,\phi_0) &= \frac{1}{\tilde{F}(0)} \sum_{\ell=1}^{L} \sum_{m=0}^{\ell} \mathscr{A}_\ell^m(r,\theta_0,\phi_0) \int_{-\infty}^{\infty} F_\ell(t) t dt \\ &= \frac{1}{\tilde{F}(0)} \sum_{\ell=1}^{L} \sum_{m=0}^{\ell} \mathscr{A}_\ell^m(r,\theta_0,\phi_0) \tau_\ell. \end{aligned} \tag{30}$$

Since $\tilde{F}(0)$ is now the area under the CIRF curve, we can state that:

$$\begin{aligned}\tilde{F}(0) &= \int_{-\infty}^{\infty} F(r,\theta_0,\phi_0,t)dt \\ &= \sum_{\ell=1}^{L}\sum_{m=0}^{\ell} \mathscr{A}_\ell^m(r,\theta_0,\phi_0)\int_{-\infty}^{\infty} F_\ell(t)dt \\ &= \sum_{\ell=1}^{L}\sum_{m=0}^{\ell} \mathscr{A}_\ell^m(r,\theta_0,\phi_0) = \mathscr{A}(r,\theta_0,\phi_0), \quad (31)\end{aligned}$$

which is called the *total amplitude* of each geomagnetic jerk. If we let:

$$\alpha_\ell(r,\theta_0,\phi_0) = \sum_{m=0}^{\ell} \frac{\mathscr{A}_\ell^m(r,\theta_0,\phi_0)}{\mathscr{A}(r,\theta_0,\phi_0)}, \quad (32)$$

then equation 30 becomes

$$\tau_1(r,\theta,\phi) = \sum_{\ell=1}^{L} \alpha_\ell(r,\theta_0,\phi_0)\tau_1(\ell). \quad (33)$$

If we use the same radial mantle conductivity model given in equation 17, but changing the parameters to $\sigma_c = 1000$ S/m and $\gamma = 3$, and taking the 1978 jerk spherical harmonic model of Le Huy *et al.* (1998), it is possible to calculate the CIRF and the delay time ($\tau_1(a,\theta_0,\phi_0)$) at a specific location. For example, by convolving the CIRF at the location corresponding to Hermanus observatory, with an assumed impulsive jerk happening at time $t = 1969$ at the CMB, the output jerk that happens at around 1974, will result in a delayed and smoothed version of the original signal (Figure 4).

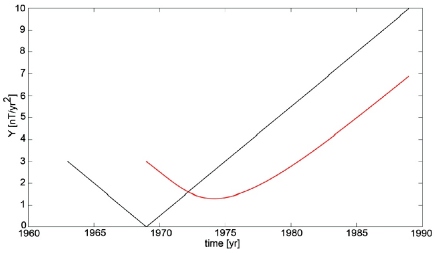

Figure 4: Example of the delay and smoothing caused by a 1D mantle conductivity given by equation 17, with $\sigma_c = 1000$ S/m and $\gamma = 3$ for the 1978 jerk spherical harmonic model given by Le Hut *et al.* (1998). The black line would be the jerk for an insulating mantle and the red line for a conducting mantle.

However, it is not possible to measure the delay time in the secular variation data because we do not know when the jerk was generated at the CMB. But one can measure what we call *differential delays* in which we choose a reference location and subtract all the other jerk occurrence times from the reference. Consequently, α_ℓ in equation 32 becomes

$$\Delta\alpha_\ell(r,\theta_0,\phi_0) = \sum_{m=0}^{\ell}\left(\frac{\mathscr{A}_\ell^m(r,\theta_0,\phi_0)}{\mathscr{A}(r,\theta_0,\phi_0)} - \frac{\mathscr{A}_\ell^m(r,\theta_{ref},\phi_{ref})}{\mathscr{A}(r,\theta_{ref},\phi_{ref})}\right), \quad (34)$$

and the differential delay times are calculated by:

$$\Delta\tau_1(r,\theta,\phi) = \sum_{\ell=1}^{L}\Delta\alpha_\ell(r,\theta_0,\phi_0)\tau_1(\ell). \quad (35)$$

Methodology: Inverse Problem

The forward problem can be summarized as: the output (jerk at the surface, $\delta\ddot{p}_\ell^m(a,t)$) is evaluated by the convolution between the input that simulates an impulsive jerk generated simultaneously (at $t = 0$) at the CMB and the Composite Impulse Response Function (CIRF, equation 28) for each jerk and location.

We followed seven main steps to solve the inverse problem:

1. Calculation of the Impulse Response Function (IRF) is performed by a modified version of Velmský and Martinec's [2005] code. The method is based on direct time-integration of the EM induction equation, and uses spatial discretization by spherical harmonics and piecewise-linear finite elements in the lateral and radial direction, respectively. The electrical conductivity is given as a piecewise constant function over layers of arbitrary thickness. Lateral variations of conductivity are neglected in this case. The boundary condition at the CMB requires prescription of the time series spherical harmonic coefficients of the vertical field. When these time series take the form of a delta function, which is numerically approximated by a narrow, zero centred and triangular function normalized to unit integral, the predicted vertical field at the Earth's surface corresponds to the product of the IRF and the geometrical attenuation $\mathscr{G}_l$.

2. Evaluation of the Composite Impulse Response Function (CIRFs, see Pinheiro & Jackson (2008) and equation 28) by using the spherical harmonic models of jerk amplitude.

3. Convolution of those CIRFs with the input jerk (Figure 1), simulated as a second order impulse in the poloidal field, simultaneous at the CMB and with unit amplitude;

4. Annual mean evaluation of the output jerk: since we aim to treat the model in the same way as the data;

5. Fitting of two straight-line segments to the output annual means by the least-squares method: the intersect is defined as the delay time (τ_1) and the error bars in τ_1 are evaluated;

6. Calculation of jerk differential delay times for all locations corresponding to the analysed observatories. The differential delay times ($\Delta\tau_1$) are calculated in relation to the mean delay value (τ_m): negative values are considered as early jerks and positive as late jerks.

7. We compare the differential delays of data with model predictions, by calculating the misfit value that is the measure of how well the differential delays of the model fit the data differential delays:

$$E = \sqrt{\frac{1}{N}\sum_{i=1}^{N}\frac{\left(\Delta\tau_{obs_i} - \Delta\tau_{mod_i}\right)^2}{\beta_{obs_i}^2}}, \quad (36)$$

where N is the number of observatories, $\Delta\tau_{obs_i}$ are the observed differential delays, $\Delta\tau_{mod_i}$ the model differential delays and β_{obs_i} the data error bars in $\Delta\tau_{obs_i}$.

Table 1: Delay times and amplitudes of two examples simulating different locations by considering harmonic degree truncation $L = 3$. For this simulation, we considered: $\tau_1(1) = 3years$, $\tau_1(2) = 2years$ and $\tau_1(3) = 1year$

Location 1

$\mathscr{A}_\ell(a,\theta,\phi)$	nT/yr^2	$\alpha_\ell(a,\theta_1,\phi_1)$	
$\mathscr{A}_1(a,\theta_1,\phi_1)$	4	$\alpha_1(a,\theta_1,\phi_1)$	0.1538
$\mathscr{A}_2(a,\theta_1,\phi_1)$	6	$\alpha_2(a,\theta_1,\phi_1)$	0.2308
$\mathscr{A}_3(a,\theta_1,\phi_1)$	16	$\alpha_3(a,\theta_1,\phi_1)$	0.6154
$\mathscr{A}(a,\theta_1,\phi_1)$	26		

Location 2

$\mathscr{A}_\ell(a,\theta,\phi)$	nT/yr^2	$\alpha_\ell(a,\theta_2,\phi_2)$	
$\mathscr{A}_1(a,\theta_2,\phi_2)$	4	$\alpha_1(a,\theta_2,\phi_2)$	-0.6666
$\mathscr{A}_2(a,\theta_2,\phi_2)$	6	$\alpha_2(a,\theta_2,\phi_2)$	-1.0000
$\mathscr{A}_3(a,\theta_2,\phi_2)$	-16	$\alpha_3(a,\theta_2,\phi_2)$	2.6666
$\mathscr{A}(a,\theta_2,\phi_2)$	-6		

In order to have a basis for comparison between different values of misfit, we define the reference misfit as:

$$E_{ref} = \sqrt{\frac{1}{N}\sum_{i=1}^{N}\frac{\left(\Delta\tau_{obs_i}\right)^2}{\beta^2_{obs_i}}} \tag{37}$$

that is the misfit for an insulating mantle model, where the differential delays are equal to zero ($\Delta\tau_{mod} = 0$). For the observatories used in the data analysis of the 1969 jerk, the reference misfit is $E_{ref} = 1.542$ considering our spherical harmonic model and $E_{ref} = 1.456$ using the model of Le Huy *et al.* (1998).

Results 1: Application of Backus mantle filter theory

We present one simple example simulating two locations with different jerk amplitudes, for some chosen delay times of each harmonic degree (Table 1). The only difference between the two examples is the amplitude of $\ell = 3$ and therefore, the α_ℓ will also change.

The IRF of each harmonic degree is represented by a PDF with mean τ_ℓ and each of these curves multiplied by the amplitudes results on the CIRF$_\ell$ while the sum of CIRF$_\ell$ over ℓ generates the total CIRF. The PDF is a good representation in location 1 where $\tau_1(a,\theta_1,\phi_1) = 1.54$ years and $\beta_2^2(a,\theta_1,\phi_1) = 1.56$ years, while in example 2 it is impossible to represent this ficticious oscillatory CIRF by a PDF since $\tau_1(a,\theta_1,\phi_1) = -1.33$ years and $\beta_2^2(a,\theta_1,\phi_1) = -8.11$ years.

In order to give a more realistic example of amplitudes we consider the 1991 jerk morphology of the East component, given by Le Huy *et al.* (1998) and the mantle radial conducting model in equation 17. The CIRFs and their approximation by PDFs (Figure 5), at locations correspondent to 10 magnetic observatories are presented as example. In some locations, as the one of Observatories 4, the delay and smoothing constants are negative and can not be represented by PDFs. If a CIRF is slightly negative for bigger time (t), negative delay and smoothing times might occurr because their integrants will enhance the negative part.

In summary, there are specific situations where Backus theory may not be applied: when the CIRF can not be approximated as PDFs and and consequently the linear relation between the electrical mantle conductivity and the delay times are not valid. That is the reason why we followed another approach in the inverse problem.

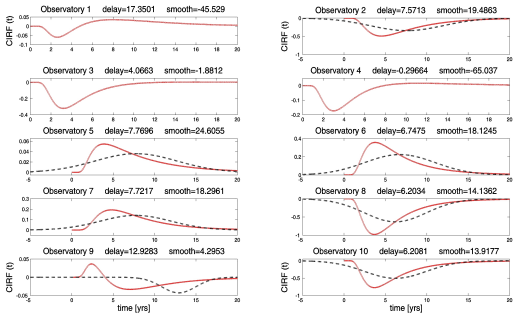

Figure 5: Composite IRF (solid line) calculated by the 1978 spherical harmonic model of Le Huy *et al.* (1998) and by considering an arbitrary model of radial electrical conductivity (equation 17). The dashed line represents the PDF approximation by using Backus' (1983) mantle filter theory for 10 locations correspondent to magnetic observatories.

Results 2: The Inverse Problem

We calculated the misfit values for the one, two and three-layer models, where for all of them we adopt the 1-D electrical conductivity model of Kuvshinov & Olsen (2006) for the first 700 km. We evaluated the IRFs for a one-layer model varying the electrical conductivity from 1000 S/m to 0.4 S/m for two jerk spherical harmonic models of the 1969 jerk amplitude (Figure 3). In both models, the misfit values increase rapidly with conductivities larger than 20 S/m and below that it oscillates in a range smaller than 0.1 of the misfit value (about 1.45 for Le Huy et al.'s (1998) model and about 1.55 by using our model).

There are only two acceptable conductivity models that are in common when using the two spherical harmonic models: $\sigma = 3$ S/m and $\sigma = 5$ S/m. By using the model from Le Huy *et al.* (1998) two more models are also smaller than the reference: $\sigma = 1$ S/m and $\sigma = 10$ S/m. Consequently, the range of acceptable models in this analysis vary from 1 S/m $\leq \sigma \leq$ 10 S/m.

In the first two-layer model we divided the lower mantle into two thick layers of 1250 km (bottom) and 950 km (top) in the low conducting range of 0.457 S/m to 12.346 S/m. The misfit values are shown in Figure 7, considering the two models of jerk amplitudes (see Figure 3). Both results show low misfit values in the range of 3 S/m for the top and bottom of the lower mantle. They also present a minima in the left top corner, which correspond to low values of conductivity in the top lower mantle (up to 1 S/m) and high values in the bottom mantle (about 12 S/m that is the maximum conductivity in this simulation). We increase the electrical conductivity values in the second simulation of a two-layer model, but considering a thin mantle layer in the bottom (300 km) that simulates the D$''$. We want to answer the question whether it is possible to have sensitivity to variations of electrical conductivity in such a thin layer in the bottom of the mantle.

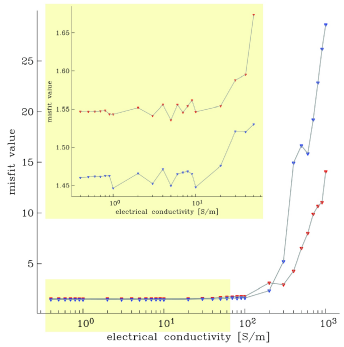

Figure 6: Misfit between the differential delays of the data and model for the one-layer mantle electrical conductivity model. We consider the spherical harmonic model of the 1969 jerk calculated in this work (red symbols) and that taken from Le Huy *et al.* (1998) (blue symbols). The plot in the top left is a zoom of the yellow area in the bigger plot.

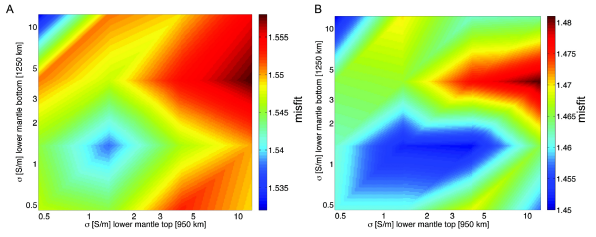

Figure 7: Misfit between the differential delays of the data and model considering the 1969 jerk spherical harmonic models from Le Huy *et al.* (1998) for the two-layer model with the mantle divided into two layers of 1250 km and 950 km.

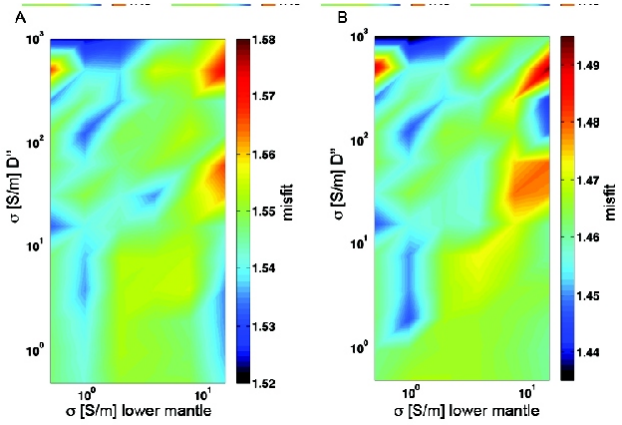

Figure 8: Misfit for the two-layer model considering the 1969 jerk spherical harmonic model calculated in this work (A) and taken from Le Huy *et al.* (1998) (B), for a higher D″ electrical conductivity and finer variations.

This result, showed in Figure 8, also suggests a low electrical conductivity for the lower mantle of about 1 S/m and a broad range of acceptable conductivities for the D″. Considering this misfit calculation, it seems the data is sensitive to variation in the thick lower mantle, but not sensitive to variations of the D″ electrical conductivity.

Conclusion

We analysed the limitations to apply Backus' (1983) mantle filter theory to constrain mantle electrical conductivity. The low frequency approximation results in the representation of the Composite IRF by a PDF, being the delay time the mean and the smoothing time, the variance. The first limitation is when the smoothing time is negative, and it can happen due to mixing of harmonics or when the delay time of each harmonic degree differs significantly. The second limitation is when one considers a high mantle electrical conductivity model and PDFs do not represent accurately the CIRFs.

The second approach to the mantle conductivity modelling was to calculate the inverse problems using the observation of geomagnetic jerks at magnetic observatories. We calculated misfit values between the differential delays measured in the data and calculated in the models of one to three layers. All simulations favour a low conductivity of the lower mantle of about 1 S/m allowing a broad range of conductivities for the D″. We believe that there is not much sensitivity of our data to detect changes in the D″ electrical conductivity.

References

Alexandrescu, M. and Gilbert, D. and Hulot, G. and Le Mouël, J-L and Saracco, G., 1996, Worldwide wavelet analysis of geomagnetic jerks, JGR, Vol. 101,B10, p21975-21994.

Backus, G. E., 1983, Application of mantle filter theory to the magnetic jerk of 1969, GJRAS, Vol. 74, p713-746.

De Michelis, P. & Tozzi, R., 2005. A local intermittency measure (LIM) approach to the detection of geomagnetic jerks, Geophys. Res. Lett., Vol. 235, p261-272.

Kuvshinov, A. & Olsen, N., 2006, A global model of mantle conductivity derived from 5 years of CHAMP, Ørsted, and SAC-C magnetic data, GRL, Vol. 33.

Le Huy, M. and Alexandrescu, M. and Hulot, G. and Le Mouël, J-L., 1998, On the characteristics of successive geomagnetic jerks, EPS, Vol. 50, p723-732.

Mandea, M., Bellanger, E., & J-L., L. M., 2000. A geomagnetic jerk for the end of the 20th century?, Earth Planet. Sci. Lett., Vol. 183, p369-373.

Nagao, H., Iyemori, T., Higuchi, T., Nakano, S., & Araki, T., 2002. Local time features of geomagnetic jerks, Earth Planets Space, Vol. 54, p119-131.

Olsen, N. & Mandea, M., 2007. Investigation of a secular variation impulse using satellite data: The 2003 geomagnetic jerk, Earth Planets Space, Vol. 255, p94-105.

Pinheiro, K. & Jackson, A., 2008, Can a 1D mantle electrical conductivity model generate magnetic jerk differential time delays? GJI, Vol. 173, 3, p781-792.

Velímský, J. & Martinec, Z., 2005. Time-domain, spherical harmonic-finite element approach to transient three-dimensional geomagnetic induction in a spherical heterogeneous earth, Geophys. J. Int., Vol. 161, p81-101.